

# Experimental investigation of BRB with transverse rib restraints

Huang Zhen<sup>1</sup>    Li Zongjing<sup>1</sup>    Ding Ting<sup>2</sup>

(<sup>1</sup>School of Civil Engineering, Southeast University, Nanjing 210096, China)

(<sup>2</sup>Jiangsu Posts & Telecommunications Planning and Designing Institute Co. Ltd, Nanjing 210006, China)

**Abstract:** To develop a high performance buckling-restrained brace (BRB) with less weight, an innovative type of the BRB with transverse rib restraints is proposed and studied through experiment. Three BRB specimens are cyclically loaded in the investigation. Specimen 1 adopts a Q235 core member and transverse rib restraints. Specimen 2 adopts a LYP160 low yield point steel core member and transverse rib restraints. Specimen 3 adopts a LYP160 low yield point steel core member and mortar restraint. The experimental results indicate that the transverse rib restraining mode can provide sufficient lateral stiffness for the core member and effectively restrain its buckling. The BRB specimens with a LYP160 core member exhibit better hysteretic performance and energy dissipation capacity than the specimens with a Q235 core member.

**Key words:** passive energy dissipation; buckling-restrained brace; low yield point steel

doi: 10. 3969/j. issn. 1003 – 7985. 2013. 01. 013

Interest in the development and application of passive control technology has greatly increased in the past two decades<sup>[1-2]</sup>. As an innovative member of passive energy dissipation, the buckling-restrained brace (BRB) usually consists of the core member, the buckle restraining member and debonding material<sup>[3]</sup>. Compared with the traditional diagonal brace, the BRB has a more stable mechanical property as shown in Fig. 1<sup>[4]</sup>. Design of the restraining structure is essential for the performance of the BRB. Large cross sections and excessive weight are defects of traditional BRBs with mortar or concrete infill restraint. This paper focuses on innovating and improving the restraining structure for less weight, smaller cross sections and better feasibility.

**Received** 2012-09-27.  
**Biography:** Huang Zhen (1975—), male, doctor, associate professor, huangzhen@seu.edu.cn.  
**Foundation items:** The National Key Technology R&D Program of China during the 12th Five-Year Plan Period (No. 2012BAJ13B01), the Science and Technology Program of the Ministry of Housing and Urban-Rural Development (No. 2011-K2-3), the Science and Technology Foundation of Southeast University (No. 9205000034), the Priority Academic Program Development of Jiangsu Higher Education Institutions (No. CE01-2-09).  
**Citation:** Huang Zhen, Li Zongjing, Ding Ting. Experimental investigation of BRB with transverse rib restraints[J]. Journal of Southeast University (English Edition), 2013, 29(1): 62 – 65. [doi: 10. 3969/j. issn. 1003 – 7985. 2013. 01. 013]

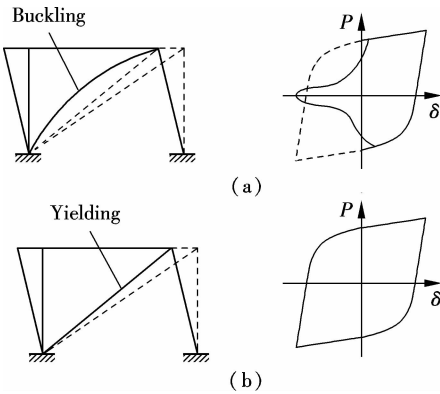


**Fig. 1** Behaviors of traditional brace and BRB. (a) Traditional brace; (b) Buckling-restrained brace

## 1 Experimental Program

### 1.1 Test specimens

Three BRB specimens are tested through the investigation. The core elements adopt Q235 plain carbon steel for specimen 1 and LYP160 low yield point steel for specimens 2 and 3. LYP160 steel has a lower yield point and better ductility than Q235 steel<sup>[5-6]</sup>. The measured section size and material properties of the core members are listed in Tab. 1. The transverse rib restraint condition is adopted for specimens 1 and 2, while the mortar restraint condition is adopted for specimen 3. The restraining ribs consist of two lines of parallel steel square tubes allocated at both sides of the core member. The cross sections of the inner square tubes are 40 mm in width and 6 mm in thickness. Gaps between the ribs are 30 mm. PTFE is used as the debonding material between the core member and the transverse ribs. Details of the structure of the BRB specimens are shown in Fig. 2, Fig. 3 and Tab. 2.

**Tab. 1** Material properties for core members

Specimen	Measured thickness	Measured width	Tensile yield strength
	$t/\text{mm}$	$w/\text{mm}$	$f_y/(\text{N} \cdot \text{mm}^{-2})$
1	9.88	89.78	237.8
2	7.58	79.02	147.6
3	8.02	80.16	147.6

### 1.2 Test setup

BRB specimens are tested using the MTS fatigue testing system. A schematic view of the experimental setup is shown in Fig. 4(a). The BRB specimens are designed to be fixed to the MTS system with end plates. During

the experiment, the BRB specimens are vertically loaded under reversed tension and compression. An overview of the test setup is shown in Fig. 4(b).

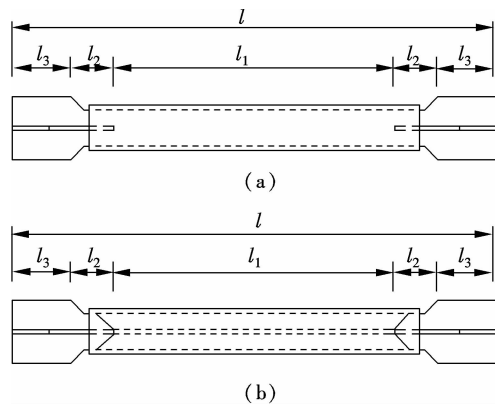


**Fig. 2** Structure of BRB specimens. (a) Front view; (b) Side view

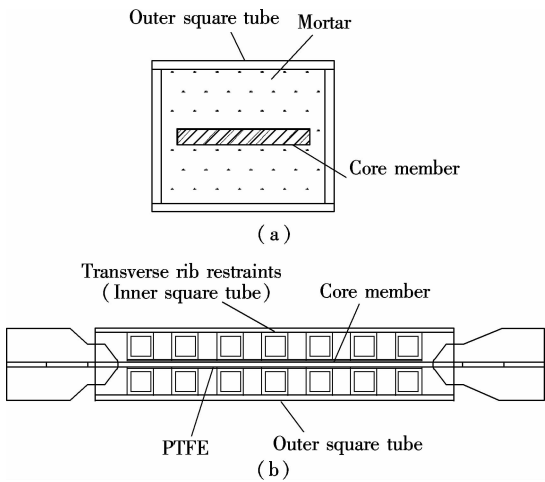


**Fig. 3** Restraining mode of BRB specimens. (a) Cross section of specimen with mortar restraint; (b) Lateral profile of specimen with transverse restraints

**Tab. 2** Geometric parameters of BRB

Specimen	Core member				Outer square tube		Restraining mode
	Steel of core member	Length of working section $l_1$ /mm	Length of transition section $l_2$ /mm	Length of connecting section $l_3$ /mm	Section size/(mm × mm × mm)	Length/mm	
1	Q235	700	80	170	122 × 160 × 8	820	Transverse ribs
2	LY160	600	95	180	130 × 130 × 8	670	Transverse ribs
3	LY160	600	95	180	140 × 140 × 8	670	Mortar

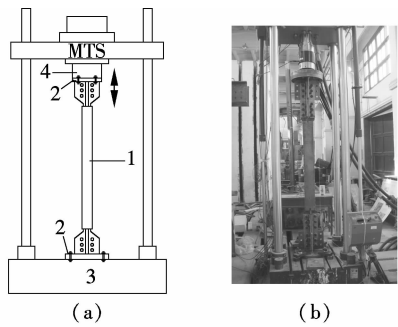


**Fig. 4** Test setup overview. (a) Schematic view; (b) Overview

1.3 Loading procedure

The BRB specimens are cyclically loaded. The loading history is determined considering the test requirements of displacement-dependent passive energy dissipation devices in “Code for seismic design of buildings” (GB 50011—2010)<sup>[7]</sup> and FEMA450<sup>[8]</sup>. Cyclic loading is controlled by the load before yielding and the displacement after yielding. Displacement loading amplitudes are  $1D_y$  to  $10D_y$ ,  $12D_y$  and  $15D_y$ , where  $D_y$  is the yield displacement of the BRB specimen, with three circles at each amplitude. Theoretical yield displacements for specimens 1, 2 and 3 are 1.01, 0.60 and 0.60 mm, respectively.

2 Test Results

The local buckling conditions of the BRB specimens are illustrated in Fig. 5. For specimens 1 and 2, local buckling of the core member occurs in the gap between

the transverse restraining elements. Hysteresis curves of the BRB specimens are illustrated in Fig. 6. Local buckling occurs in specimen 1 at  $12D_y$ , while local buckling occurs in specimen 2 at  $15D_y$ . Among the three specimens, specimen 2 and specimen 3 obtain full and more stable hysteresis curves, which indicates that the low yield point steel applied in the core member is beneficial to the hysteresis performance of BRB. Experimental yield displacements for specimens 1, 2 and 3 are 1.03, 0.65 and 0.65 mm, respectively, which match well with the theoretical yield displacement.

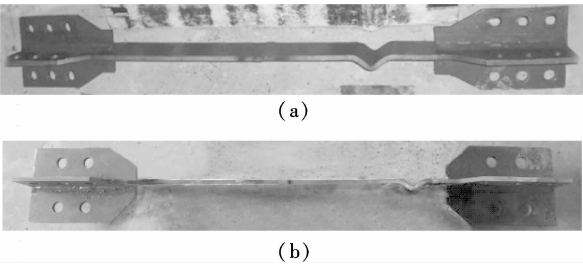


**Fig. 5** Failure condition of BRB specimens. (a) Specimen 1; (b) Specimen 2

3 Evaluation of Hysteresis Performance

3.1 Difference of tensile and compressive load

Due to the friction between the core member and the restraining member under compression loading, the axial compressive load tends to be greater than the axial tensile load. The percentage of tensile and compressive difference is calculated as

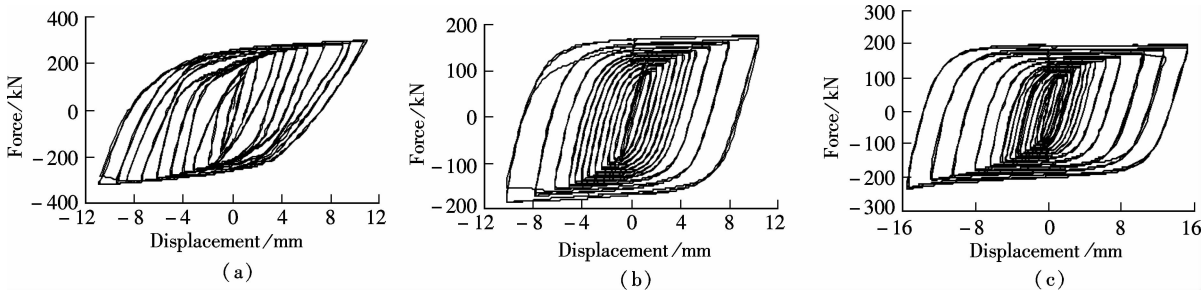


**Fig. 6** Hysteresis curves of cyclic loading tests. (a) Specimen 1; (b) Specimen 2; (c) Specimen 3

$$R = \frac{(|P^-| - |P^+|)}{0.5(|P^-| + |P^+|)} \times 100\% \quad (1)$$

where  $R$  is the percentage of tensile and compressive difference;  $P^-$  and  $P^+$  are the maximum axial compressive load and maximum axial tensile load at the same am-

plitude of displacement, respectively. Taking specimen 2 for example, the tensile and compressive differences are obtained from cyclic loading results, as shown in Tab. 3, where  $D_y = 0.6$  mm.

According to Ref. [9], the difference of tensile and

**Tab. 3** Tensile and compressive axial load difference of specimen 2

Displacement	$D_y$	$3D_y$	$5D_y$	$7D_y$	$9D_y$	$10D_y$	$12D_y$	$15D_y$
$ P^+ /\text{kN}$	84.21	110.97	122.12	136.32	144.2	148.28	156.63	167.87
$ P^- /\text{kN}$	82.05	113.42	124.89	139.85	149.08	155.2	166.56	184.6
$R/\%$	-2.57	2.21	2.27	2.59	3.38	4.67	6.34	9.97

compressive axial force shall not exceed 30%. As can be seen from Tab. 3, the tensile and compressive differences of the axial load of specimen 2 increase gradually as the axial displacement increases, but the percentages of the tensile and compressive difference are all within 30% throughout the loading process, which meets the requirements of relevant standards.

**3.2 Energy dissipation indices**

According to FEMA356<sup>[10]</sup>, hysteresis performance indices of the displacement-dependent energy dissipation device mainly include effective stiffness  $K_{\text{eff}}$  and equivalent damping ratio  $\zeta_{\text{eq}}$ , as shown in Fig. 7.

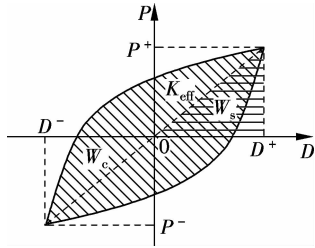


**Fig. 7** Energy dissipation indices

For practical use, it is sometimes preferable to express BRB properties in an equivalent viscous system. This is basically a single degree of freedom oscillator with an effective stiffness  $K_{\text{eff}}$  defined as

$$K_{\text{eff}} = \frac{|P^+| + |P^-|}{|D^+| + |D^-|} \quad (2)$$

where  $D^+$  and  $D^-$  are the maximum tensile and compressive displacement, respectively;  $P^+$  and  $P^-$  are the axial forces corresponding to  $D^+$  and  $D^-$ , respectively. The damping ratio  $\zeta_{\text{eq}}$  for the equivalent system is defined as

$$\zeta_{\text{eq}} = \frac{W_c}{4\pi W_s} \quad (3)$$

where  $W_c$  is the area enclosed by a complete hysteresis loop, which represents the energy dissipated in a cycle, and  $W_s$  is the area of a triangle, which represents the energy stored in an elastic spring with a stiffness  $K_{\text{eff}}$  and a displacement  $D^+$ .

The relationship between  $K_{\text{eff}}$  and displacement ratio ( $D/D_y$ ) is shown in Fig. 8.  $K_{\text{eff}}$  decreases as the displacement ratio increases. The reason for the degradation of  $K_{\text{eff}}$  is due to the increase of plastic deformation after the yielding of the core member. Theoretical results are

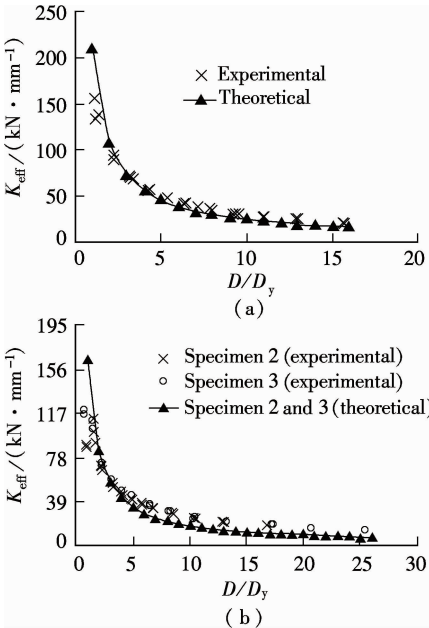


**Fig. 8** Effective stiffness. (a) Specimen 1; (b) Specimens 2 and 3

obtained by finite element analysis with the same parameters using the bilinear model. As can be seen from Fig. 8, test results agree with the theoretical results.

As shown in Fig. 9, when the displacement ratio reaches higher than 3, specimens 2 and 3 provide a damping ratio in excess of 30%. Specimens 2 and 3 with a LYP160 core member obtain higher values of equivalent damping ratio  $\zeta_{eq}$  than specimen 1 with a Q235 core member. Besides, specimens 2 and 3 match better with the theoretical curve than specimen 1. Therefore, the results indicate that the energy dissipation capacity of BRB with a LYP160 core member is better than that of BRB with a Q235 core member.

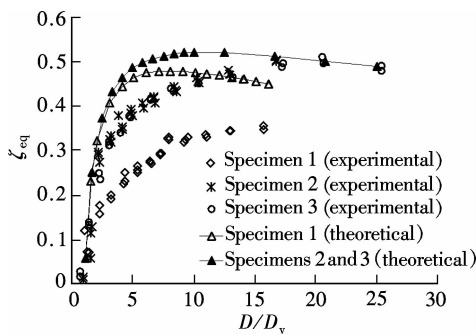


Fig. 9 Equivalent damping ratio

#### 4 Conclusions

1) Specimen 2 exhibits full hysteresis curves with the equivalent damping ratio in excess of 30% at a large displacement range, and the percentages of tensile and compressive difference are all within 30%, which indicates a good energy dissipation performance of the BRB with transverse rib restraints.

2) The specimen with a LYP160 core member exhibits better hysteretic performance than the specimen with the Q235 core member, which indicates that low yield point steel applied in the core member is beneficial to the hysteretic performance of BRB.

3) Transverse rib restrained BRB can achieve the same level of hysteretic performance with mortar restrained BRB, but much lighter than the latter one, and more convenient for production, which verifies the credibility and advantage of the transverse rib restrained BRB.

#### References

- [1] Housner G W, Bergman L A, Caughey T K, et al. Structural control past, present, and future [J]. *Journal of Engineering Mechanics*, 1997, **123**(9): 897–971.
- [2] Soong T T, Spencer B F. Supplemental energy dissipation: state-of-the-art and state-of-the-practice [J]. *Engineering Structures*, 2002, **24**(3): 243–259.
- [3] Xie Q. State-of-the-art of buckling-restrained braces in Asia[J]. *Journal of Construction Steel Research*, 2005, **61**(6): 727–748.
- [4] Tsai K C, Hwang Y C, Weng C S. Seismic performance and applications of double-tube buckling-restrained braces [J]. *Progress in Steel Building Structures*, 2005, **7**(3): 1–8. (in Chinese)
- [5] Saeki E, Sugisawa M, Yamaguchi T, et al. Mechanical properties of low yield point steels [J]. *Journal of Materials in Civil Engineering*, 1998, **10**(3): 143–152.
- [6] Wen D H, Song F M, Liu Z C, et al. Manufacture and application of low yield point steel used for earthquake resistance [J]. *Progress in Steel Building Structures*, 2009, **11**(5): 16–19. (in Chinese)
- [7] Ministry of Housing and Urban-Rural Construction of People's Republic of China. GB 50011—2010 Code for seismic design of buildings [S]. Beijing: China Architecture & Building Press, 2010. (in Chinese)
- [8] Federal Emergency Management Agency. FEMA 450 NEHRP recommended provisions for seismic regulations for new buildings and other structures [S]. Washington DC, USA: Federal Emergency Management Agency, 2004.
- [9] AISC/SEAOC. Recommended provisions for buckling-restrained braced frames [S]. AISC/SEAOC, 2001.
- [10] Federal Emergency Management Agency. FEMA 356 Prestandard and commentary for the seismic rehabilitation of buildings [S]. Washington DC, USA: Federal Emergency Management Agency, 2000.

## 横肋约束防屈曲支撑试验研究

黄 镇<sup>1</sup> 李宗京<sup>1</sup> 丁 婷<sup>2</sup>

(<sup>1</sup> 东南大学土木工程学院, 南京 210096)

(<sup>2</sup> 江苏省邮电规划设计院有限责任公司, 南京 210006)

**摘要:**为研发轻质高性能防屈曲支撑(BRB),提出了一种新型横肋约束防屈曲支撑并对其进行了试验研究。对3组BRB试件进行了低周往复加载试验。试件1采用普通Q235钢核心单元,并采用横向加劲肋约束;试件2采用LYP160低屈服点钢核心单元,并采用横向加劲肋约束;试件3采用LYP160低屈服点钢核心单元,并采用砂浆约束。试验结果表明,横向加劲肋可以为核心单元提供足够的侧向刚度,有效抑制核心单元的屈曲。采用LYP160低屈服点钢核心单元的BRB试件比采用普通Q235钢核心单元的BRB试件表现出更好的滞回性能和更强的耗能能力。

**关键词:**被动耗能减震;防屈曲支撑;低屈服点钢

**中图分类号:** TU352.1